Electronic Supplementary Material (ESI) for Soft Matter.

Supplementary Information

Rapid dynamics of cell shape recovery in response to local deformations

Kristina Haase[1], Tyler N. Shendruk[2], and Andrew E. Pelling[1,3,4]

Supplementary Methods

Cell culture.

HeLa cells were cultured at 37°C and 5% CO_2 in DMEM with 10% heat inactivated fetal bovine serum and 1% penicillin (100 IU/mL), streptomycin (100 1g/mL) (Hyclone). Cells were cultured on 100 mm dishes (Corning) and seeded onto 35 mm glass bottom dishes (laser-cut 35mm plastic culture dishes (TPP) affixed with 1.5 glass 25mm round coverslips (Harvard apparatus Canada) using PDMS (Dow Corning)), in 2.5 ml of culture media.

Plasmids and transfections.

HeLa cells were cultured on 35 mm glass bottom dishes to ~60% confluency before transfections. Plasmids (~0.6 μg) for the PH domain of PLC-δ conjugated to EGFP (kind gift of Guillaume Charras) and LifeAct-Ruby (kind gift of Buzz Baum) were diluted in OptiMEM (Invitrogen) as described previously [1]. The transfection complex was completely removed and replaced with culture medium 45 min later. Experiments were performed the following day. Immediately prior to the experiment, Hoechst 33342 (Invitrogen) was used to stain DNA, according to manufacturer specifications.

Drug treatments.

Cells were pre-treated in a cell culture incubator at 37°C and 5% CO_2 immediately before experiments. Cells were pre-treated for 30 min with either the rho-kinase inhibitor Y-27632 (10 μM in DMSO, Sigma) or the microtubule depolymerizer Nocodazole (Noco) (10 μM in DMSO, Sigma), or pre-treated for 15 min with the actin destabilizing drug Cytochalasin-D (CytD) (10 μM in DMSO, Sigma). In some cases, cells were pre-treated with Y-27632 for 15 min followed by subsequent treatment with Noco for 15 min.

In order to deplete cholesterol levels, methyl-β-cyclodextrin (MβCD), a cyclic oligosaccharide, was used (10 mM diluted in dH_2O, Sigma). Cells were incubated with MβCD for 30 min at 37°C and 5% CO2 in serum-free media followed by washing twice with PBS and complete media change. Considering that MβCD was dissolved in a large volume of dH_2O, we used a control population where cells from the same passage were incubated with serum-free medium and the equivalent ratio of dH_2O (~500 μL MβCD solution added to 2 mL media) for 30 min.

Immunochemistry.

Cells were fixed using 3.5% paraformaldehyde and permeabilized using 0.5% v/v Triton X-100 at 37°C. Cells were then stained for actin using Alexa Fluor 546 Phalloidin (Invitrogen), and DNA using DAPI

(Invitrogen). Microtubules were stained with a mouse monoclonal anti-α-tubulin (Abcam) primary antibody followed by an Alexa Fluor 488 rabbit anti-mouse immunoglobin (Invitrogen) secondary antibody. Full details have been described previously [2].

Image acquisition.

All images, for live and fixed cells, were acquired with a Nikon TiE A1-R high-speed resonant laser scanning confocal microscope (LSCM), using a 60x (NA = 1.2) water immersion objective lens. Appropriate laser lines and filter sets were employed; GFP was excited using a 488 nm laser and measured at 525 nm, and RFP was excited using a 561 nm laser with fluorescence measured at 595 nm. Fixed samples were imaged using LSCM volumes in galvano scanning mode. Imaging of live cell experiments were performed in resonant scanning mode. In this mode, LSCM volume images were captured prior-to and during deformation experiments, and consisted of ~30 confocal planes, each 0.5 μm thick. Time-lapse images were performed in a single XY-plane in order to capture the intensity decrease/increase due to deformation/recovery of the cell, at a scan rate of 7.69 fps. To reduce noise, line averaging (2x) was used.

Confocal resolution.

To determine the confocal resolution of GFPs and RFPs used herein, we employed green and red fluorescent (200nm) carboxylate-modified microspheres (Invitrogen) diluted in dH_2O to a final concentration of 10^6, as outlined previously [3]. A 20 µl drop of the diluted stock solution was pipetted onto a clean 1.5 glass coverslip and allowed to dry overnight. LSCM imaging of microspheres was performed the following day with the same excitation wavelength ($\lambda_{exc} = 488$ nm for a 525 nm emission, and $\lambda_{exc} = 561$ nm for 595 nm emission) and sampling rate (0.069 x 0.069 x 0.18 µm) used during experiments. Here, we based our theoretical confocal resolution on the Rayleigh criterion [3, 4]:

$$\text{Lateral resolution} = \frac{0.51\,\lambda_{exc}}{NA} \qquad [S1]$$

$$\text{Axial resolution} = \frac{0.88\,\lambda_{exc}}{\left(n - \sqrt{n^2 - NA^2}\right)} \qquad [S2]$$

Based on equations (1, 2), (using n=1.33 for water) the theoretical resolution for GFP was calculated to be 207 nm in x and y, and 567 nm in z. Theoretical resolution for RFP was calculated as 238 nm in x and y, and 652 nm in z. Using an ImageJ plugin, MetroloJ (the plugin and manual can be found: //imagejdocu.tudor.lu/doku.php?id=plugin:analysis:metroloj), we were able to generate a report of the miscrosphere PSF data. Fits of microsphere intensity to a Gaussian equation were used to determine the FWHM. This produced a mean resolution of: 0.248 in x µm, 0.281 µm in y, and 0.701 µm in z for GFP microscpheres (n=10). Mean confocal resolution was lower for RFP microspheres (n=10): 0.305 µm in x, 0.351 µm in y, and 1.043 µm in z.

Atomic force microscopy.

A NanoWizard II (JPK Instruments) AFM was mounted on the LSCM to perform integrated AFM-LSCM experiments. All experiments were performed at 37°C, using a temperature-controlled AFM stage (JPK).The thermal fluctuation method of Hutter and Bechhoefer was used to calibrate AFM tips [5]. The

sensitivity and stiffness was measured prior to experiments. All AFM cantilevers had an experimentally determined stiffness, k = 0.08 ± 0.01 N/m (PNP-TR triangular, Nanoworld). Young's modulus (E) was determined by recording force-curves measured over the center of cell nuclei. A shallow region (200 nm) of indentation was fit to the Hertz model for a conical tip [6] to measure local E of the cell (PUNIAS Software) [7].

Stiffness measurements for MβCD-treated cells were performed on two controls: cells treated with MβCD in serum-free media, as well as cells treated with the addition of the same concentration of dH_2O to normal DMEM (see Fig. S6b).

Deformation and recovery experiments.

First, LSCM volume images were recorded prior to and following deformation experiments to ensure cells recovered their initial shape (Fig. S2). Next, tracking of membrane-cortex deformation and recovery involved capturing images in a single XY-plane set approximately 2 μm below the apical region of the membrane (as determined by LSCM volume images) (Fig. 1, main text). To capture the initial deformation, images were recorded prior to (~5 s) and during 20 s of constant force application. The AFM cantilever was set to approach the sample rapidly (10 μm/s), with forces of either 10 or 20 nN applied above the approximate center of cell nuclei (visualized by Hoechst).

A similar method was used to examine the dynamics of cell shape recovery. A series of constant force (10 nN) experiments were performed for varied durations: 15 s, 1 min, or 10 min. Again, time-lapse imaging was performed in a single XY-plane during the retraction phase of the tip (following the specified load duration). For long durations (1 and 10 min), LSCM volume images were acquired once every minute. For instance, a 10 nN force was applied at the approximate center of the cell for 10 min, during which 11 LSCM volume images were taken corresponding to t=0 (before indentation), t=1 (indentation after 1 min) and so on, up to t=10 minutes of applied force. Following force application, the focal plane is manually set to ~2 μm below the apical membrane. As the AFM tip is retracted, continuous XY-plane time-lapse images are acquired to capture the recovery of the membrane/cortex (~30 s). Following this, a final LSCM volume image was captured (t≈12 min).

Statistics.

Statistics were calculated using two sample t-tests. Where indicated, one-way ANOVA analyses with post-tests including Levene's test for equal variance, and a means comparison test using the Bonferroni and Tukey methods were employed. Unless otherwise noted, all significance indicates $P < 0.050$.

Image analysis of deformation/recovery profiles.

ImageJ (open-source image processing software, http://rsbweb.nih.gov/ij/) was used for all analysis. A square region of interest (ROI) (0.69 μm^2) was chosen; one containing the deformed cell membrane and cortex. Brightness and contrast settings were adjusted in order to optimize images of live and fixed cells. No other image manipulations were performed. In order to examine the deformation dynamics of the membrane and cortex, time-lapse images were analyzed by capturing mean intensity over time within the ROI (Fig. 1c, main text). Deformation experiments (Fig. 1b) were normalized by averaging initial intensity values observed within the ROI 2 seconds prior to unloading. A value of I=1 represents the

maximum intensity immediately prior to deformation (t=0), and I=0 the average minimum intensity after the AFM tip is extended. For recovery experiments, I=0 occurs during the deformation while the AFM tip is approached. Following tip retraction, the intensity within the ROI increases as the membrane/cortex pass the imaging plane (maximum normalized to I=1).

Non-linear regression of intensity during deformation.

We chose to fit the deformation intensity profiles to a first-order decay, based on Akaike's (AIC) and Bayesian (BIC) information criteria (Origin v.9.1) [8]. Non-linear regression of intensity-time profiles allowed us to compare decay rates (τ (s)) of the membrane and cortex using equation [S3].

$$I(t) = I_o + Ae^{-t/\tau} \quad \text{[S3]}$$

Using normalized intensity data, the offset, I_o, was set to zero, and the amplitude, A, was set to 1. The only free fit parameter was τ, a characteristic decay rate.

Measuring cellular strain.

Approximate axial strain measurements were made on cells during long (1 and 10 min) deformation experiments, as we previously reported [1]. Axial strain was measured in the plane of loading, as:

$$\varepsilon = d/h_o \quad \text{[S4]}$$

where d is the deformation and h_o is initial cell height. An average of the two measurements were made from orthogonal projections of LSCM volume images.

Derivation of viscoelastic model of relaxation/recovery.

Here, we propose a simple model for the dynamics and recovery of the membrane/cortex based on the telegraph equation. First, consider a series of masses (m) connected by Hookian springs (with spring constants K_1) separated by a horizontal distance ℓ (Fig. 4a, main text). In the deformed state at a time t after the tip is removed, these masses are displaced from equilibrium and the i^{th} mass is displaced by a height u_i^t. This mass is acted upon by the spring force of its neighbours and so is accelerated. Equating the total inertial force to the Hookian spring forces and taking the continuum limit produces the wave equation for an elastic membrane.

Any additional forces that couple the membrane and cortex to the subcellular environment can now be superimposed onto each element causing the simple wave equation to generalize into a form of the telegrapher equation. Here, we employed forces from a single elastic (K_2) and damping (γ) element in parallel acting on each element. Since the elastic and viscous contributions act in parallel, this amounts to a Kelvin-Voigt viscoelastic model and the net force on each element of the surface is then the sum of an elastic and a viscous dissipation term. The resulting telegrapher equation is

$$m\frac{\partial^2 u_i^t}{\partial t^2} = K_1\left[u_{i+1}^t - 2u_i^t + u_{i-1}^t\right] - K_2 u_i^t - \gamma\frac{\partial u_i^t}{\partial t}$$

By once again taking the continuum limit of $\ell \to 0$ as $N \to \infty$ such that $L = N\ell$ is finite and definite the speed of wave propagation $c = \sqrt{K_1\ell^2/m}$, we find

$$0 = \frac{\partial^2 u(\vec{r},t)}{\partial t^2} - c^2 \nabla^2 u(\vec{r},t) + \frac{K_2}{m} u(\vec{r},t) + \frac{\gamma}{m} \frac{\partial u(\vec{r},t)}{\partial t} \quad [S5]$$

In this form, the above equation can be described as a surface connected to equilibrium by elements of the Kelvin-Voigt model. Comparing to equation [2] in the main text, we see that $k = K_2/mc^2$ and $\mu = \gamma/mc^2$ with units of μm^{-2} and s·μm^{-2}, respectively. In the final form of equation [S5], we neglect the inertial term by assuming that we are in the over-damped regime and will not observe inertial dynamics on the membrane surface. We expect a monotonic return to equilibrium, which is reasonable considering that the cell is surrounded by viscous fluid and is largely composed of cytoplasm.

Numerical implementation of the viscoelastic model calculation.

Equation [S5] does not have an analytic solution and so is solved numerically. The AFM tip is modelled as a cylindrically symmetric cone defined by a solid angle $\Omega = 35°$ and a maximum indentation depth h. An implicit Euler method was found to be stable and employed to determine the displacement u_i^t at all radial points and times. Non-dimensionalized variables were used in this process. The characteristic length scale was identified to be the maximum displacement h, the characteristic time is μh^2. In the following, all variables are non-dimensionalized by these scales. The assumed cylindrical symmetry and over-damped dynamics causes equation [S5] to reduce to

$$0 = \frac{1}{r} \frac{\partial}{\partial r} \left[r \frac{\partial u(r,t)}{\partial r} \right] - \mu \frac{\partial u(r,t)}{\partial t} - k u(r,t) \quad [S6]$$

Applying the implicit Euler method for the spatial derivatives and evaluating them at the future time $t+1$, discretizes equation [S6] into the form

$$u_i^t = \left[\frac{a}{r_i} - b \right] u_{i-1}^{t+1} + [1 + d + 2b] u_i^{t+1} - \left[\frac{a}{r_i} + b \right] u_{i+1}^{t+1} \quad [S7]$$

where $a = \Delta t/(2\Delta r)$, b= $\Delta t/(\Delta r)^2$ and $d = k\Delta t$. Equation [S7] holds for all discretization nodes except at the boundaries. The assumed cylindrical symmetry demands a von Neumann boundary condition at the centre i.e. $u_{i-1}^{t+1} = u_i^{t+1}$ at $i = 0$. We assume a Dirichlet boundary condition of $u_i^{t+1} = u_i^t$ at the last node $i = N$. All of this can be written concisely in the form $\vec{u}^t = \boldsymbol{A}\vec{u}^{t+1}$, where $\vec{u}$ is the list of displacements at each node and $\boldsymbol{A}$ is the invertable tridiagonal matrix defined by inspection of Equation [S7]. Because $\boldsymbol{A}$ can be numerically inverted using standard algorithms, the Euler method can calculate all the future displacements from the current displacements via $\vec{u}^{t+1} = \boldsymbol{A}^{-1}\vec{u}^t$.

Measurements of intensity profiles do not directly measure displacement height; rather they infer changes in height from the measured intensity at the focal plane, which lies at a depth $f \approx 2$ μm below the equilibrium surface $u = 0$ in the ROI. To estimate the intensity, we assume that fluorescence occurs homogeneously and constantly on the apical membrane. Since the emitted photons must transverse the dispersive intracellular medium to arrive at the focal plane, we approximated the intensity at each point by a Gaussian dispersion about the focal plane. In this way, the total intensity is the integral of the intensity at each point on the focal plane in the ROI. Furthermore, we estimate the intensity at each point to be the integral of the Gaussian dispersion with a variance σ^2 from each point on the membrane

as given by the displacement equation [S7]. This is done numerically, with cylindrical symmetry and with a numerical cut-off of $r_{cut} = 100h$, used in integrating the intensity at each point in the ROI. In this way, the experimental intensity as a function of time was predicted.

Experimental parameters, such as the maximum tip depth h, the focal plane f, and the dispersion σ^2 (an optical property that may vary substantially between fluorescent protein expression levels), all vary between experiments. Therefore, these parameters must be prescribed using best estimates, or as fitting parameters along with the viscoelastic properties of interest, k and μ. In our fitting procedure, the average value $h = 5$ μm (~maximum deformation range (see Table S3)), $\sigma = 0.2$ μm (approximate theoretical x-y resolution of GFP) and an ROI radius of 0.469 μm are set for all fits. The number of radial nodes is set to $N = 500$, the radial step size is $\Delta r = 0.06$ μm and the time step used is $\Delta t = 100$ μs. The position of the focal plane f, the elastic constant k and viscous coefficient μ are fit using an iterative least-squares method. This routine is then repeated until the step sizes for f, k and μ are all less than the prescribed tolerance of $\varepsilon = 10^{-5}$.

Supplementary Tables

Table S1 | Load magnitude and duration do not affect recovery. Mean recovery constants are displayed following short and long (durations and different load magnitudes. One-way ANOVA analysis with both Tukey and Bonferroni post-tests demonstrated no significant change. Variance was significantly different between populations (Levene's test, $P < 0.05$). "Top" refers to measurements made at the most apical region of the cell (Fig. S3). Values shown are means ± SD. * indicates $P < 0.05$,

			Membrane		Cortex	
Load	Duration	N	κ_1 (s^{-1})	κ_2 (s^{-1})	κ_1 (s^{-1})	κ_2 (s^{-1})
10 nN	15 s	8	2.66 ± 1.04	0.08 ± 0.06	2.84 ± 0.60	0.05 ± 0.01
	1 min	14	2.35 ± 1.04	0.07 ± 0.06	2.41 ± 1.00	0.07 ± 0.04
	1 min (top)	9	1.86 ± 1.01	0.05 ± 0.03	0.64 ± 0.36*	0.06 ± 0.03
	10 min	11	2.52 ± 1.22	0.08 ± 0.12	2.21 ± 1.13	0.05 ± 0.04
20 nN	15 s	6	2.41 ± 0.94	0.05 ± 0.05	1.53 ± 0.73	0.03 ± 0.01
	1 min	13	2.91 ± 0.54	0.28 ± 0.43	2.83 ± 0.64	0.09 ± 0.05
	10 min	11	3.04 ± 0.96	0.15 ± 0.17	2.36 ± 1.09	0.07 ± 0.07

Table S2 | Cytoskeletal and osmotic effects on shape recovery. Characteristic recovery constants of the membrane and cortex are shown following a 1 min 10 nN load. "Top" refers to measurements made at the most apical region of the cell (Fig. S3). Values shown are means ± SD. * indicates $P < 0.05$, and ** indicates $P < 0.08$, in comparison to untreated cells under the same condition (see Table S1).

			Membrane		Cortex	
	Duration	N	κ_1 (s^{-1})	κ_2 (s^{-1})	κ_1 (s^{-1})	κ_2 (s^{-1})
CytD	15 s	6	0.69 ± 0.97*	0.03 ± 0.02	0.28 ± 0.13*	0.02 ± 0.01
	1 min	12	1.24 ± 1.10*	0.05 ± 0.04	0.98 ± 1.08*	0.05 ± 0.02*
	10 min	6	0.12 ± 0.06*	0.00 ± 0.02	0.10 ± 0.02*	0.01 ± 0.01*
Y-27632	15 s	10	1.12 ± 0.87*	0.08 ± 0.05	0.88 ± 0.58*	0.06 ± 0.03
	1 min	13	1.22 ± 1.10*	0.10 ± 0.11	0.85 ± 0.82*	0.07 ± 0.06
	10 min	15	0.89 ± 1.27*	0.01 ± 0.05	0.89 ± 1.29*	0.03 ± 0.04
Noco	15 s	6	0.88 ± 0.98*	0.04 ± 0.02	0.63 ± 0.74*	0.04 ± 0.03
	1 min	11	1.52 ± 1.56	0.04 ± 0.03	1.50 ± 1.48	0.04 ± 0.01
	10 min	8	1.36 ± 1.54	0.02 ± 0.02	1.24 ± 1.21	0.04 ± 0.01
300 mM Sucrose	1 min	7	0.18 ± 0.08*	0.02 ± 0.02**	0.16 ± 0.06*	0.08 ± 0.10
30% dH_2O	1 min	12	1.58 ± 1.19*	0.10 ± 0.23	1.66 ± 1.22*	0.07 ± 0.11

Table S3 | Cytoskeletal and osmotic effects on deformation. Direct measurements of initial height (h_o), deformation (d), and approximate axial strain (d/h_o) are shown for cells following 1 min of 10 nN force (unless otherwise noted). Values shown are means ± SD. * Indicates significance ($P < 0.05$).

	N	h_o, height (μm)	d, deformation (μm)	ε, axial strain (%)
Untreated (10nN)	20	7.62 ± 1.24	3.73 ± 1.35	50 ± 19
Untreated (20nN)	20	8.07 ± 2.35	5.04 ± 1.23*	66 ± 19*
CytD	18	9.38 ± 1.41*	6.45 ± 1.18*	69 ± 13*
Y-27632	20	9.70 ± 1.85*	6.36 ± 1.21*	66 ± 09*
Noco	11	7.09 ± 1.42	4.13 ± 1.24	58 ± 12
300 mM Sucrose	9	4.41 ± 2.26*	1.46 ± 0.89*	32 ± 12*
30% dH_2O	17	10.08 ± 1.62*	3.61 ± 1.26	37 ± 13*

Table S4 | Viscoelastic characterization of shape recovery. Shown are mean elastic and viscous components of recovery curves modeled by equation [S3]. Reported κ_r is average k/μ cacluated for paired simulations. *Indicates significant difference with untreated HeLa (10nN) ($P < 0.05$, using t-test). Values shown are means ± SD.

	N	k (μm^{-2})	μ ($s \cdot \mu m^{-2}$)	$\kappa_r = k/\mu$ (s^{-})
Untreated (10nN)	8	125.01 ± 64.34	68.08 ± 84.94	7.17 ± 6.64
Untreated (20nN)	12	120.49 ± 74.55	62.33 ± 66.09	5.32 ± 6.56
CytD	8	58.98 ± 135.08	141.80 ± 118.51	2.77 ± 7.60
Y-27632	17	3.89 ± 3.94	71.82 ± 49.27	*0.06 ± 0.03
Noco	4	203.19 ± 341.74	703.79 ± 547.43	8.03 ± 15.98
30% dH_2O	13	132.22 ± 64.34	143.98 ± 171.71	5.61 ± 9.48

Table S5 | Osmotic change affects shape recovery. Membrane and cortex recovery constants (κ) are shown for various epithelial cells. Values shown are means ± SD. $^{+}$ Notes that only N=4 of 5 for Y+N and Y+N + 30% dH_2O, N=11 of 20, and N=4 of 10 datasets were successfully fit for untreated and MβCD-treated cells, respectively. Fast recovery resulted in discontinuities in intensity curves (thus the mean value is an under-estimate). *Indicates significance with respect to neutrally osmotic Y+N-treated cells, $P < 0.02$.

		Membrane		Cortex		Membrane	
	N	κ_1 (s^{-1})	κ_2 (s^{-1})	κ_1 (s^{-1})	κ_2 (s^{-1})	h_o, height (μm)	ε, axial strain (%)
Y-27632 + Noco (Y+N)	4^{+}	0.38 ± 0.41	0.10 ± 0.08	0.71 ± 0.29	0.09 ± 0.04	9.68 ± 2.09	15 ± 10
Y+N + 30% dH_2O	4^{+}	2.33 ± 0.54*	0.37 ± 0.48	2.18 ± 1.15	0.21 ± 0.20	13.08 ± 1.70*	29 ± 5*
Untreated	11^{+}	2.52 ± 1.22	0.08 ± 0.12	2.21 ± 1.13	0.05 ± 0.04	10.3 ± 2.9	50 ± 18
MβCD	4^{+}	2.42 ± 0.58	0.03 ± 0.01	2.17 ± 0.41	0.04 ± 0.02	8.8 ± 1.8	40 ± 11

Table S6 | Recovery of non-cancerous epithelial cells. Membrane and cortex recovery constants (κ) are shown for various epithelial cells. Values shown are means ± SD.

		Membrane		Cortex	
	N	κ_1 (s^{-1})	κ_2 (s^{-1})	κ_1 (s^{-1})	κ_2 (s^{-1})
MDCK	21	1.73 ± 1.10	0.11 ± 0.09	1.11 ± 0.82	0.13 ± 0.09
HEK	16	2.51 ± 0.94	0.09 ± 0.06	1.17 ± 1.08	0.09 ± 0.03
CHO	4	3.52 ± 0.17	0.21 ± 0.13	1.72 ± 0.59	0.07 ± 0.03

Supplementary Figures

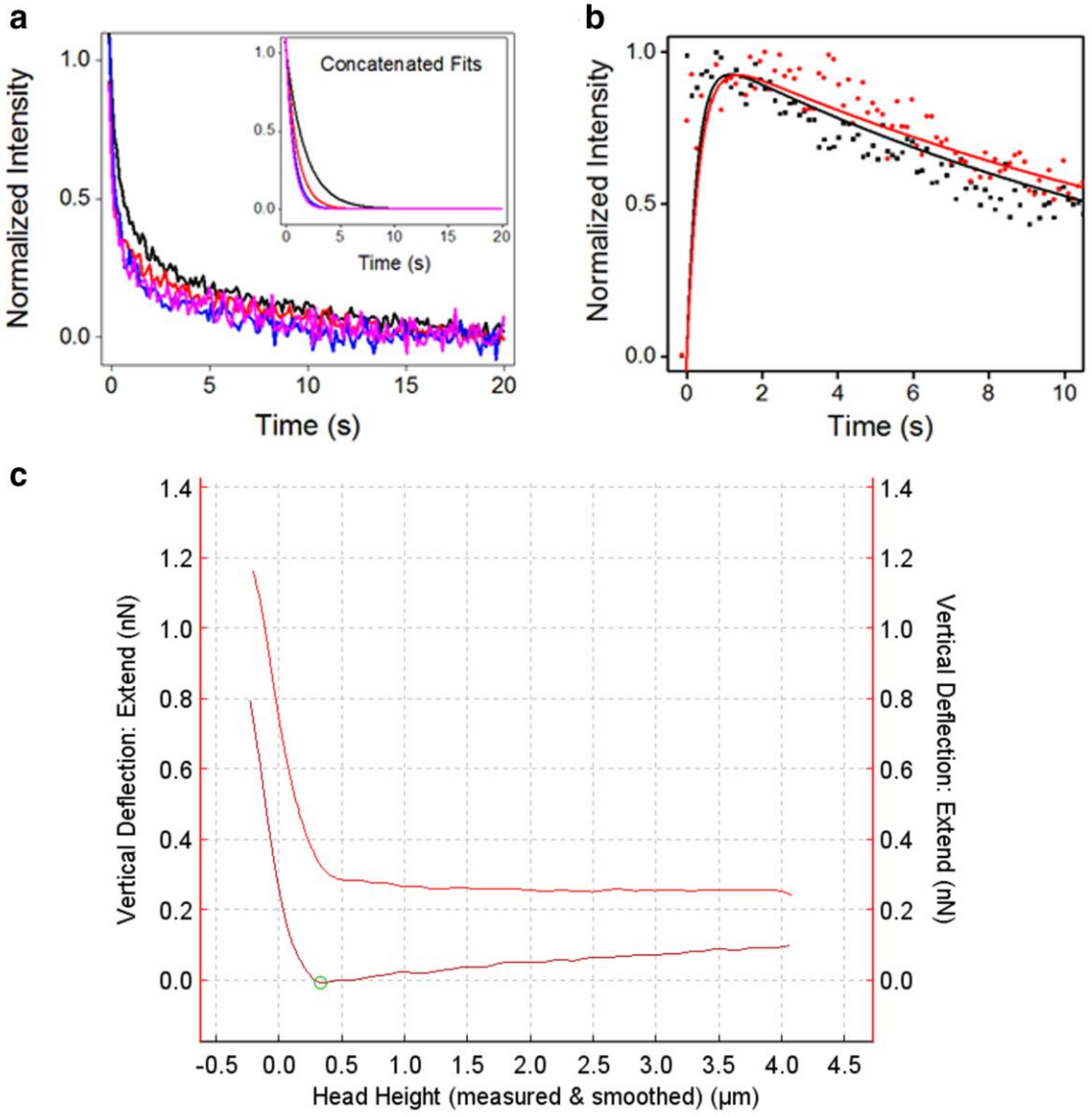

Figure S1 | Membrane and cortex deform and recover simultaneously. a, Normalized plots of intensity over time are shown for the initial 20 s of membrane (n=13, black – 10 nN, blue – 20 nN) and cortex (n=7, red – 10 nN, magenta – 20 nN) deformations following approach of the AFM tip (t=0). Curve variances were significantly different (P = 0.04). *Inset* Concatenated fits to an exponential decay were compared between the membrane τ = 1.78 ± 0.04 s and cortex τ = 1.04 ± 0.03 s (10 nN decay rates) (P > 0.05, and F=0.70). Due to the rapid cantilever approach speed (10 µm/s), varying load magnitude (10 to 20 nN) did not significantly alter the observed response of the membrane or cortex (P > 0.05). **b**, Fits of normalized recovery curves are shown overlaying raw data for an untreated HeLa cell following a 10 nN load applied for 1 min. No significant differences appeared between characteristic times or fits between membrane and cortex or load magnitudes (P > 0.05, using paired t-tests and F-test for fits comparison). **c**, Typical AFM force-curve demonstrating insignificant adhesion between tip and cell (6.9 pN, green

circle, measured using JPK SPM Data processing software). The majority (n=10/12) of cells demonstrated adhesion forces orders of magnitude lower than the rate of force retraction during multiple approach-retract curves.

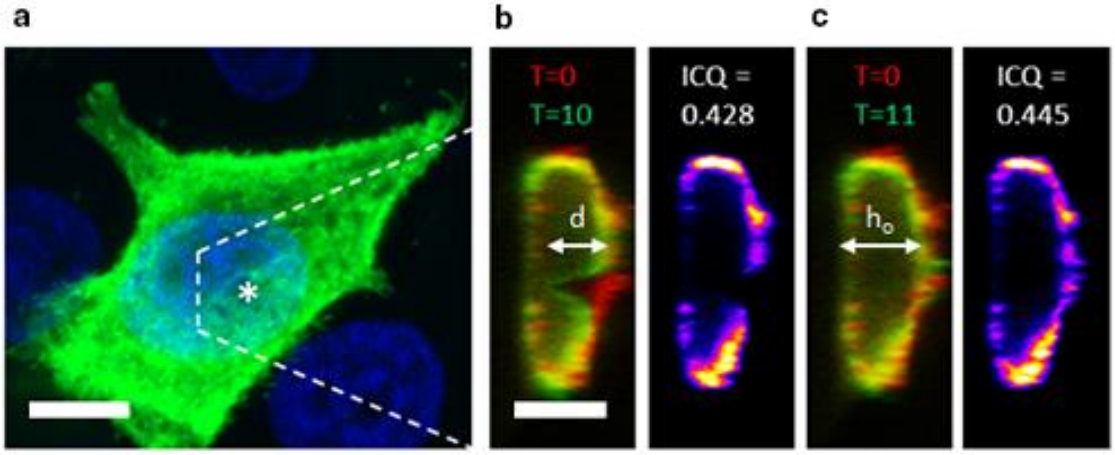

Figure S2 | Cell shape recovery following large deformations. a, Z-projection of a HeLa cell deformed by a 10 nN constant force applied for 10 min. **b-c**, Shown are red /green overlays of orthogonal projections and corresponding intensity correlation analysis (ICA) and quotients (ICQ). **b**, Deformation (d) following 10 min of applied force is **c**, recovered, measured in relation to initial height (h_o), following 1 min of force cessation. Positively correlated intensities (bright colours) and increased ICQ values are shown following tip retraction. See reference [9] for details on ICA. Scale bars are 10 µm.

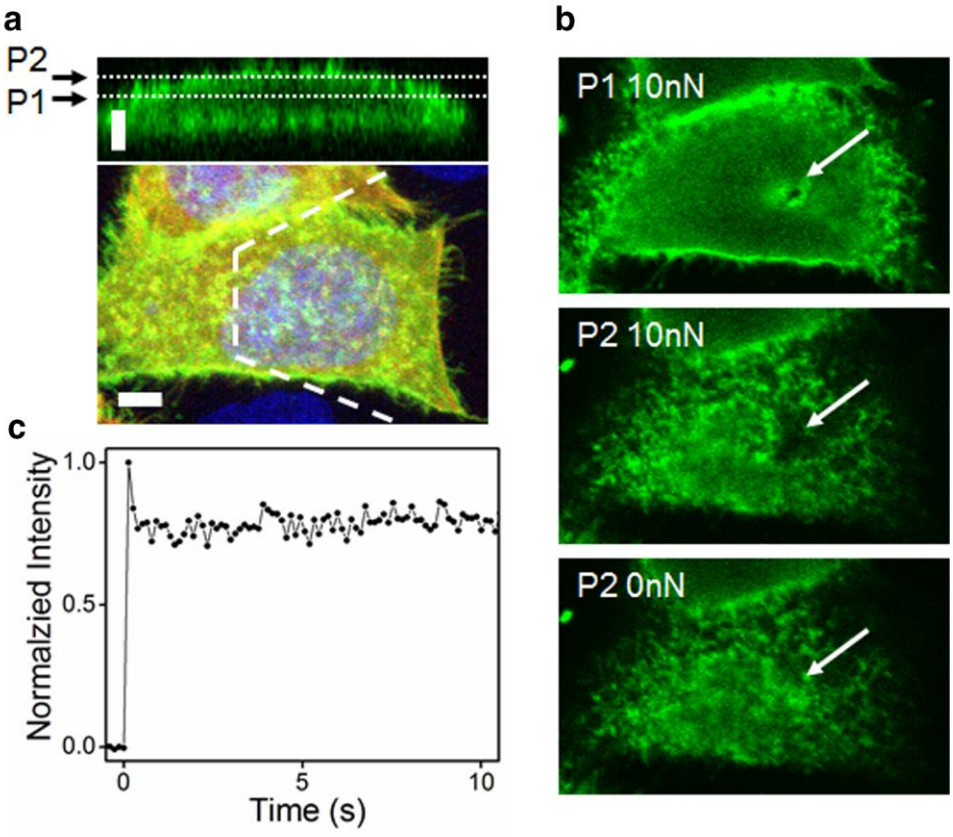

Figure S3 | Imaging plane does not affect recovery. **a**, LSCM image of a HeLa cell with XZ projection demonstrating the continuous imaging planes P1, ~2 µm below apical membrane, and P2, at the apical region. **b**, XY-images during tip approach demonstrating differences in visible deformations corresponding to P1 and P2 in (**a**). Arrow indicates deformed region. Scale bars are 5 µm. **c**, Intensity profile acquired during continuous imaging in P2 after 10 nN load removal. Sharp intensity peak demonstrates near-instantaneous recovery.

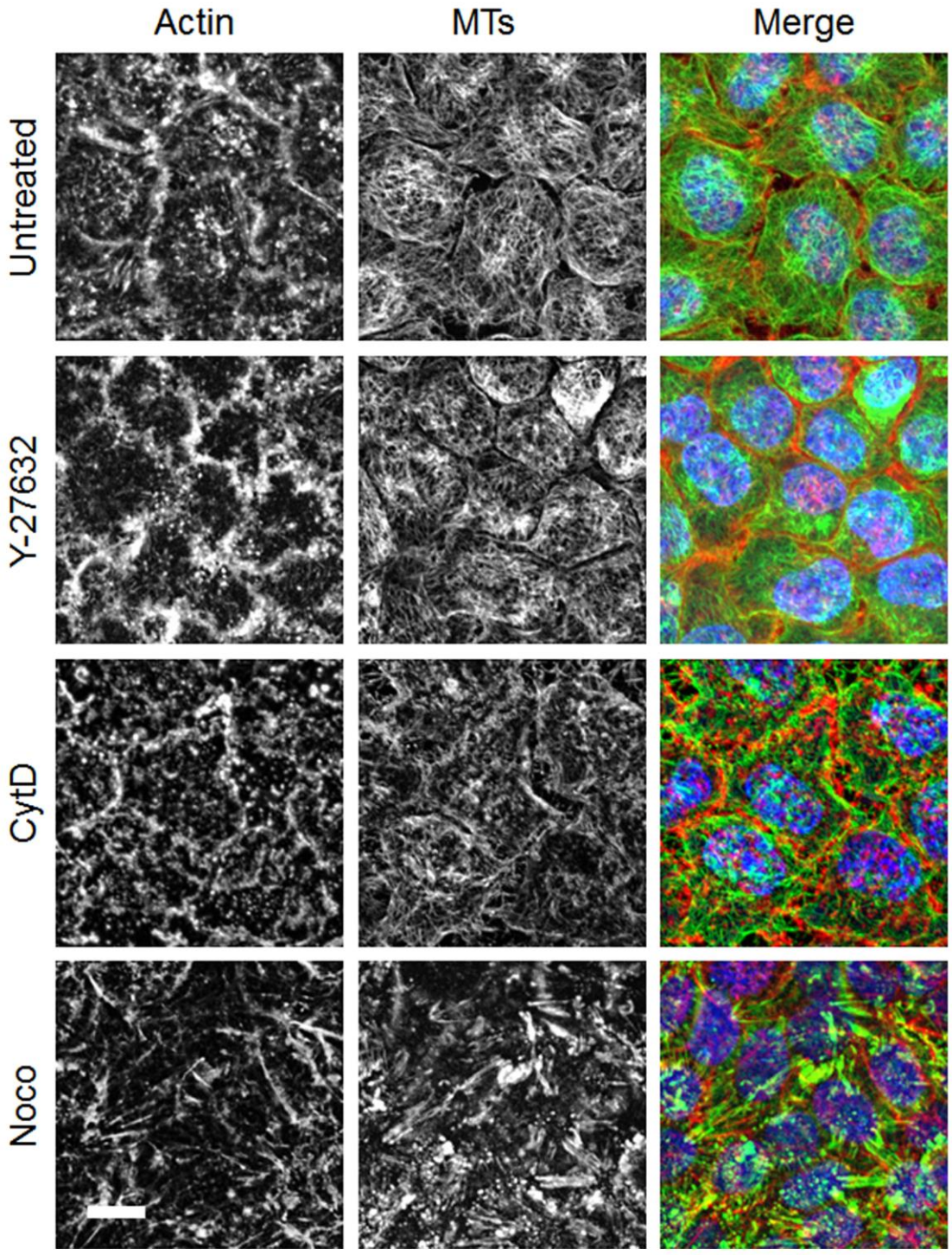

Figure S4 | Cytoskeletal disruption by inhibitors. Immunofluorescent images of fixed cells demonstrate differences in cytoskeletal morphologies following treatment with inhibitors. Scale bar is 10µm.

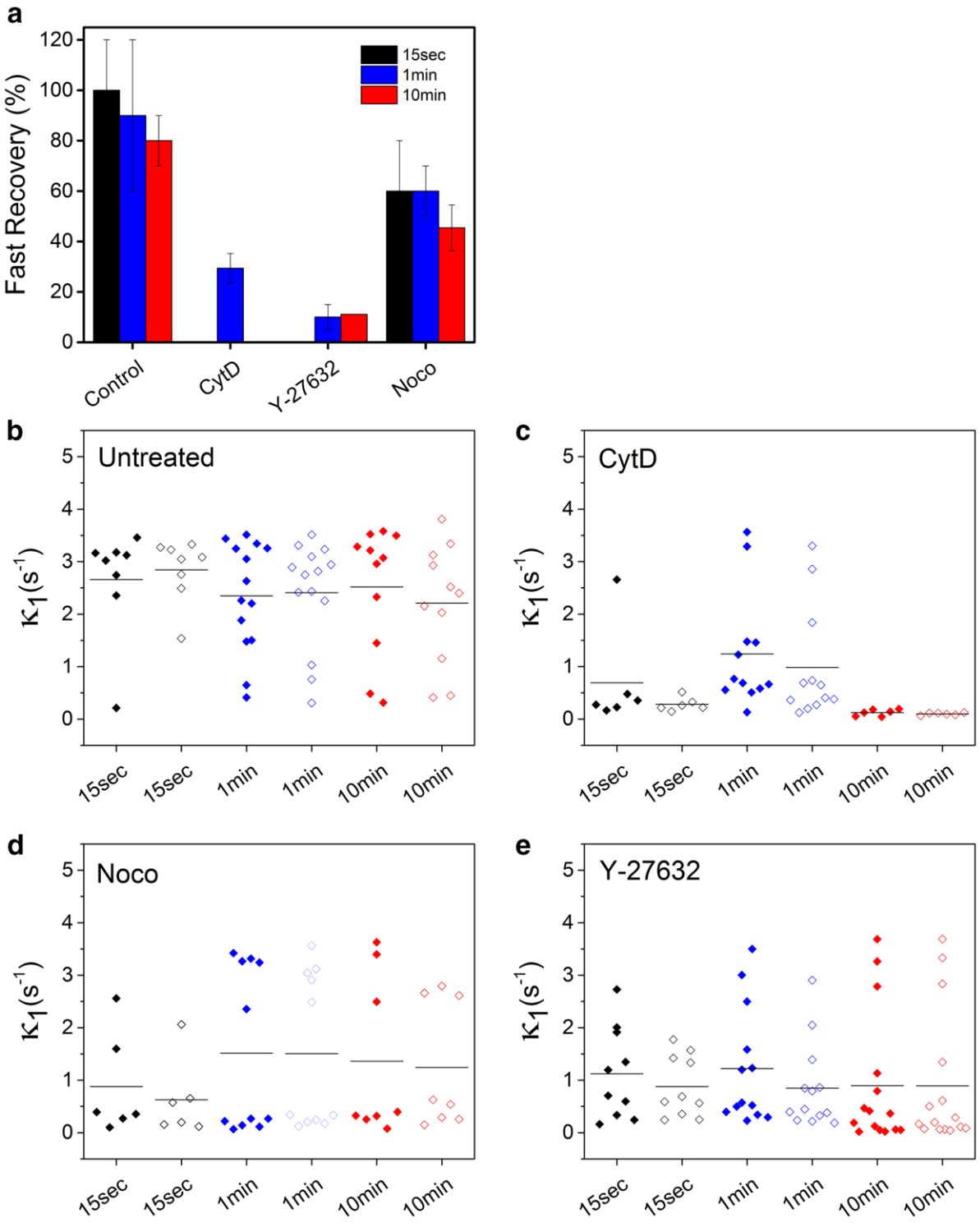

Figure S5 | Cell shape recovery is time-independent. a, Percentage of fast recovering cells, as measured from membrane videos (see Table S1 and S2 for n values). Error is difference between membrane and cortex. **b-d,** Raw data distributions of decay constants (κ_1) from membrane (solid) and cortex (hollow) recovery curves. There is no significant difference ($P > 0.05$) between paired membrane and cortex fits

(t-tests), or between varied durations for any of the untreated or treated cases as measured by one-way ANOVA, and post-hoc Tukey test. Only for the case of Noco-treated cells is there a difference in variance between durations (Levene's test).

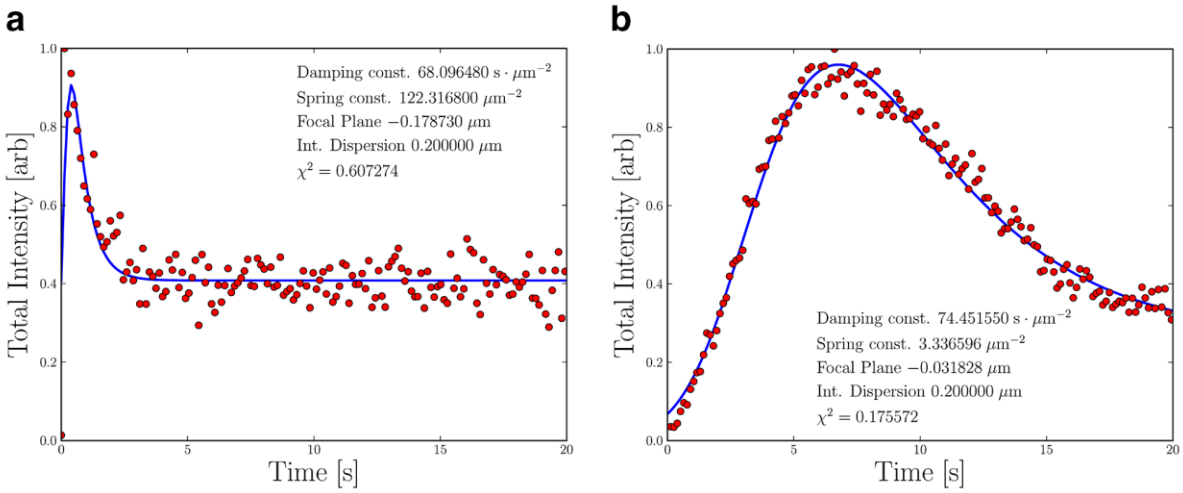

Figure S6 | Simulation of recovery using viscoelastic model. Example outputs from the viscoelastic simulation (equation 2, main text) of a HeLa cell undergoing **a**, fast recovery, and **b**, slow recovery following 1 min of 10 nN. Fits, shown in blue, overlay the normalized intensity data (red).

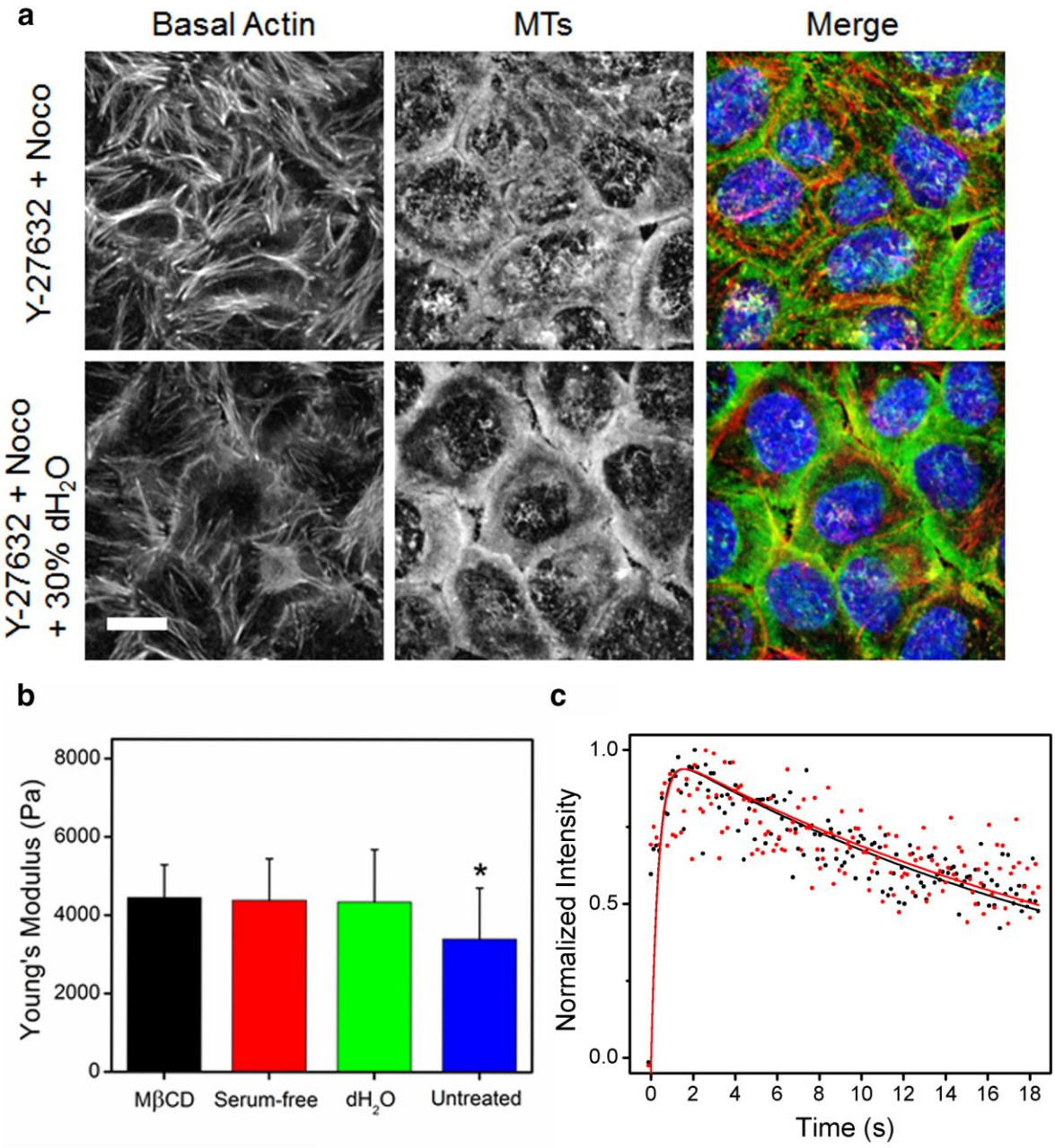

Figure S7 | Osmotic pressure dictates stiffness and recovery. a, Images of fixed cells demonstrate differences in cytoskeletal morphologies following hypo-osmotic shock of Y-27632+ Noco treated HeLa. Scale bar is 10µm. **b**, Young's modulus measurements from AFM force-curves. Shown are mean ± SD. * Indicates significance in comparison to all other conditions ($P < 0.05$, with paired t-tests). **c,** Fit of normalized recovery curves shown overlaying raw data for an untreated cell (black) and MβCD-treated (red) cell following a 10 nN load applied for 10 min. No significant differences appeared between fits ($P > 0.05$, using paired t-tests and F-test for fits comparison).

References

1. Haase K, Pelling AE. Resiliency of the Plasma Membrane and Actin Cortex to Large-Scale Deformation. Cytoskeleton (Hoboken) 2013; 70:494-514.
2. Pelling AE, Veraitch FS, Chu CPK, Mason C, Horton MA. Mechanical Dynamics of Single Cells During Early Apoptosis. Cell Motil Cytoskel 2009; 66:409-22.
3. Cole RW, Jinadasa T, Brown CM. Measuring and interpreting point spread functions to determine confocal microscope resolution and ensure quality control. Nat Protoc 2011; 6:1929-41.
4. Beyer H. Handbuch der Mikroskopie. VEB Verlag Technik, 1985.
5. Hutter JL, Bechhoefer J. Calibration of Atomic-Force Microscope Tips. Rev Sci Instrum 1993; 64:1868-73.
6. Matzke R, Jacobson K, Radmacher M. Direct, high-resolution measurement of furrow stiffening during division of adherent cells. Nat Cell Biol 2001; 3:607-10.
7. Carl P, Kwok CH, Manderson G, Speicher DW, Discher DE. Forced unfolding modulated by disulfide bonds in the Ig domains of a cell adhesion molecule. P Natl Acad Sci USA 2001; 98:1565-70.
8. Motulsky H. Fitting Models to Biological Data Using Linear and Nonlinear Regression: A Practical Guide to Curve Fitting: A Practical Guide to Curve Fitting. Oxford University Press, 2004.
9. Li Q, Lau A, Morris TJ, Guo L, Fordyce CB, Stanley EF. A syntaxin 1, G alpha(o), and N-type calcium channel complex at a presynaptic nerve terminal: Analysis by quantitative immunocolocalization. J Neurosci 2004; 24:4070-81.